Eur. Phys. J. D (2017) 71: 31
DOI: 10.1140/epjd/e2016-70603-9

THE EUROPEAN PHYSICAL JOURNAL D

Regular Article

Resonance effects in near-threshold electron-impact excitation of the 143.4 nm line in the Pb^+ ion*

Anna N. Gomonai[a], Yuriy I. Hutych, and Aleksandr I. Gomonai

Department of Electron Processes, Institute of Electron Physics, Ukrainian National Academy of Sciences, 21 Universitetska str., 88017 Uzhgorod, Ukraine

Received 28 September 2016 / Received in final form 6 December 2016
Published online 14 February 2017 –

Abstract. Electron-impact excitation of the resonance transition $6s^2 6d\ ^2D_{3/2} \rightarrow 6s^2 6p^2 P^o_{1/2}$ (143.4 nm) in the Pb^+ ion within the (6–100) eV energy range is studied spectroscopically using a crossed-beam technique. The observed distinct structure in the energy dependence of the effective excitation cross section (including the energy region above the ion ionization potential) is primarily due to the decay of atomic and ionic autoionizing states, produced mainly by excitation of an electron from the subvalence $5d^{10}$ shell, to the resonance levels (directly or via the cascade transitions). The absolute cross section value for the line under investigation was determined by normalizing the experimental curve at the electron beam energy of 100 eV to the theoretical data obtained by the Van-Regemorter formula and found to be $(0.5 \pm 0.3) \times 10^{-16}$ cm^2.

1 Introduction

Precise experimental measurements of electron-impact excitation of heavy ions are essential for many different applications including diagnostics of the temperature and density of emitting plasma, the abundances of elements within the plasma as well as development of optical atomic clocks, testing theories, research of atomic structure and applications in astrophysics [1]. A detailed investigation of high-resolution astrophysical spectra requires a large number of accurate atomic data [2]. In addition, lead has been identified in different astrophysical objects. With an ionization potential of 15.0 eV, Pb II is the dominant form of lead in the neutral interstellar medium. For example, the $6s^2 6d\ ^2D_{3/2} \rightarrow 6s^2 6p\ ^2P^o_{1/2}$ transition of the Pb^+ ion at 143.4 nm was detected in the emission spectra of several stars [3,4]. Additional detections of the Pb^+ ion λ143.4 nm line are available in archival Space Telescope Imaging Spectrograph data [5].

The active experimental and theoretical studies by different scientific teams on the electron-impact excitation, ionization, and electron-ion recombination of ions (see, e.g., Ref. [1]) have shown that an important role is played by the resonance processes (resonance excitation and dielectronic recombination) related to the formation and multichannel decay of autoionizing states of the "electron + ion" system. Resonance phenomena strongly affect the cross sections of all electron-ion collision processes, especially in the near-threshold region, which appear to be a very important additional scattering channel in different plasmas. The threshold region is very important in both fusion and astrophysics: cross sections and electron energy distribution functions have their maxima at the threshold, thereby resulting in a large excitation rate at the threshold. Study of the resulting resonances gives a valuable information on the dynamics of the scattering processes and should represent a test for theoretical calculations.

Our previous studies of the In^+ [6–8] and Tl^+ [9] ions with filled subvalence $(n-1)d^{10}$ shell and valence ns^2 shell showed that in these cases the resonance processes are substantially complicated due to the inter-shell interaction and relativistic effects. The Pb^+ ion is in the same row of the Periodic Table as the Tl^+ ion which showed a significant contribution of resonance processes to the electron-impact excitation cross-sections. With the filled $5d^{10}$ and $6s^2$ inner shells and outer $6p$ shell, the Pb^+ ion is an important example of complexity of core-valence correlation, relativistic effects including the Breit interaction, and strong configuration mixing. Additionally, full understanding of scattering phenomena related to both structure and dynamics of the Pb^+ ion is an important step in modeling complex multi-electron ions. Unfortunately, no data are available so far regarding the inelastic process cross-sections at the interaction of electrons with Pb^+ ions, except for the work [10] where the theoretical calculations and experimental crossed-beam measurements for electron-impact single ionization of Pb^{q+} ions for $q = 1$–10 are compared.

* Contribution to the Topical Issue "Many Particle Spectroscopy of Atoms, Molecules, Clusters and Surfaces", edited by A.N. Grum-Grzhimailo, E.V. Gryzlova, Yu V. Popov, and A.V. Solov'yov.

[a] e-mail: annagomonai@gmail.com

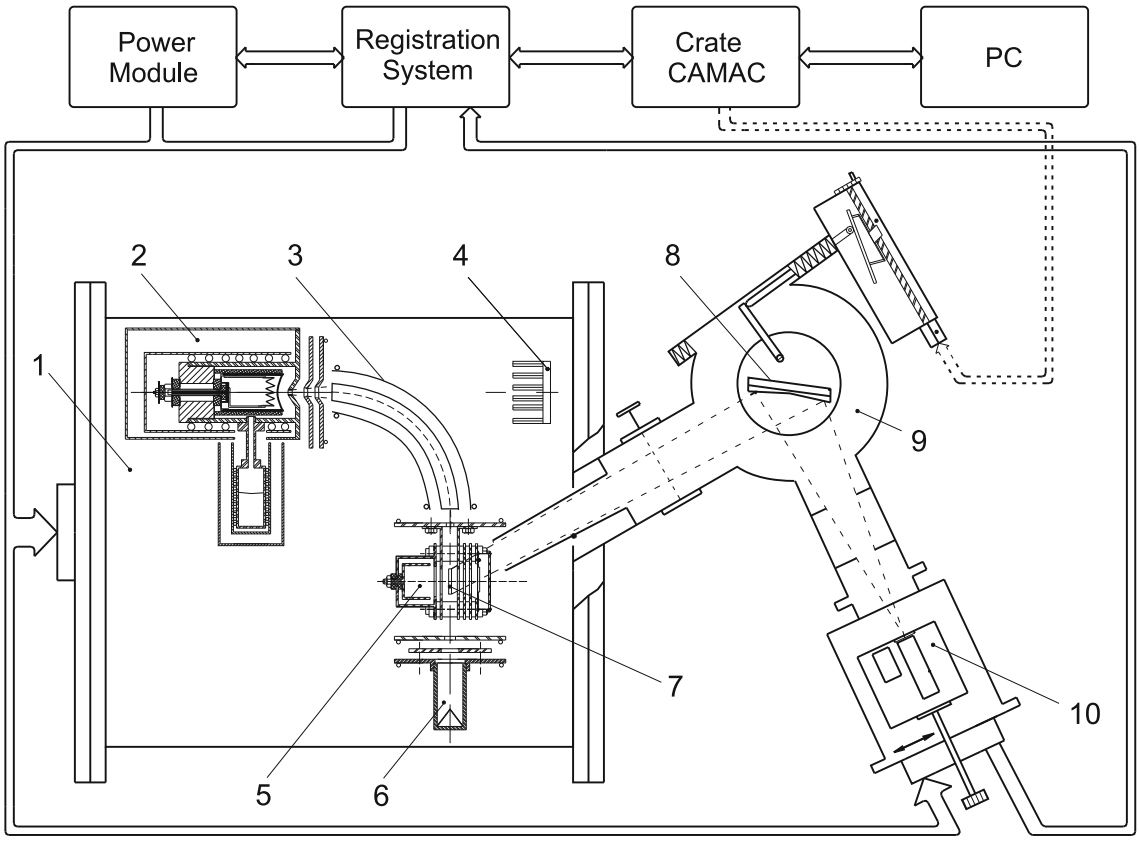

Fig. 1. Schematic layout of experimental setup: 1 – vacuum chamber, 2 – ion source, 3 – electrostatic ion selector, 4 – cooled atom trap, 5 and 6 – deep Faraday cups, 7 – electron gun, 8 – diffraction grating, 9 – vacuum monochromator, 10 – cooled solar-blind photomultiplier.

Here we present the results on the electron excitation effective cross-section measurements of the transition $6s^2 6d\ ^2D_{3/2} \rightarrow 6s^2 6p\ ^2P^o_{1/2}$ (λ143.4 nm) in the Pb^+ ion:

$$e + Pb^+(6s^2 6p)\ ^2P^o_{1/2} \rightarrow Pb^{+*}(6s^2 6d)\ ^2D_{3/2} + e' \downarrow Pb^+(6s^2 6p)\ ^2P^o_{1/2} + h\nu. \quad (1)$$

2 Experimental procedure

The experimental procedure included bombardment of target Pb^+ ions by electrons with controlled energy and detection of photons emitted by the excited Pb^+ ions. The schematic of the experimental setup is shown in Figure 1. The crossed-charged-beam apparatus and the technique applied were described in detail in our earlier studies [6,7]. Here we discuss some main aspects of the method trying to restrict the detailed discussions to the issues specific for the present experiment.

The features of the ion source design intending to produce single-charged lead ions in the ground state were described in detail elsewhere [6]. The ion beam current in the collision region was $(0.5–1.0) \times 10^{-6}$ A at the Pb^+ ions energy 800 eV. The ion beam was reproducible and stable with the relative uncertainty better than 0.5% for the operating period of about 300 h.

The ions are bombarded by a ribbon electron beam in the equipotential interaction region. The electron beam current in the energy region of E_e = (6–100) eV was $(5–50) \times 10^{-5}$ A and the energy spread (FWHM) of the electron beam was 0.6 eV.

The electron energy scale was calibrated using the excitation threshold of the λ121.6 nm line of atomic hydrogen by electron impact:

$$e + H_2 \rightarrow H(1s\ ^2S) + H(2p\ ^2P) + e' \quad H(2p\ ^2P) \rightarrow H(1s\ ^2S) + h\nu\ (\lambda 121.6\ \text{nm}). \quad (2)$$

The spectroscopic threshold for producing Lyman-alpha photons is 14.67 eV [11]. The measurement was done at a variety of electron beam currents and both with and without the Pb^+ ion beam traversing the collision volume. This allowed us to take into account the influence of the space charge of the crossed charged beams.

The true electron-beam energy in the collision region was also determined using the energy calibration formula [12]:

$$eV_e = e\left(V_c - \phi - \frac{S_e I_e}{V_e^{1/2}} + \frac{S_i A_i^{1/2} I_i}{V_i^{1/2}}\right) \quad (3)$$

where V_c is the cathode potential, ϕ is the cathode contact potential, I_e and I_i are the electron and ion currents, V_i is the ion acceleration voltage, A_i is the ion atomic weight, S_e and S_i are geometrical constants, $(S_e/V_e^{1/2})I_e$ describes the retarding effect, resulting from the electron beam space charge depression of the on-axis potential in the collision region, $(S_i A_i^{1/2}/V_i^{1/2})I_i$ describes the ion space-charge acceleration effect, i.e. the influence of the ion beam space charge on the electrons as they approach the ion beam. The procedure of the electron energy scale calibration was described in details earlier [7]. The discrepancy between the two methods of the true electron energy determination did not exceed 0.1 eV. The accuracy of the electron energy scale calibration was ±0.1 eV.

The photon detection system comprised a 70° VUV monochromator, a photomultiplier, and an electronic detection system. The monochromator is based on the Seya-Namioka scheme with a concave toroidal grating (50 × 40 mm^2 working area with 1200 grooves/mm) and has an inverse linear dispersion $d\lambda/dl \approx 1/7$ nm/mm. The radiation was detected by a cooled solar-blind FEU-142 photomultiplier. The dark count of the photomultiplier was typically 0.2 counts/s. The photomultiplier sensitivity was stable within 3%. A four-way chopping scheme was used in order to separate the signal due to the inelastic process under investigation from the large background count rate resulting from the interactions of both beams with the residual gas. The desired signal rates of (0.5–1.2) counts/s were extracted at the signal-to-background ratio of 1/10 to 1/20. The beam currents and photon signals were accumulated for 1000 s with typically from 5 to 10 times per data point. The data reproducibility was ensured by measurement performed at maximally controlled and stable experiment parameters and was verified in numerous measurements under various experimental conditions.

The spectral sensitivity of the detection system was determined by measuring the emission intensities of the nitrogen atom spectral lines in the VUV range by electron impact on N_2 with the electron energy of 100 eV. The procedure of determination of the detection system spectral sensitivity was described in detail earlier [7].

The experimental errors were dominated by the statistical uncertainties of counting. All statistical uncertainties were quoted at the confidence level of 68% corresponding to the mean standard deviation. The different errors were judged to be uncorrelated and the total uncertainties were calculated as indirect measurement errors. The total error of determination of the absolute emission cross-section value was estimated to be 65%.

3 Results and discussion

The results of the precise experimental investigation of electron-impact excitation of the radiative transition from the $6s^2 6d\ ^2D_{3/2}$ level to the $6s^2 6p\ ^2P^o_{1/2}$ level (λ143.4 nm) are shown in Figure 2. The bars at the points represent the relative uncertainty at the 68% confidence level. The uncertainty of the relative emission excitation cross sections was evaluated to be ±10 %. Vertical bars indicate

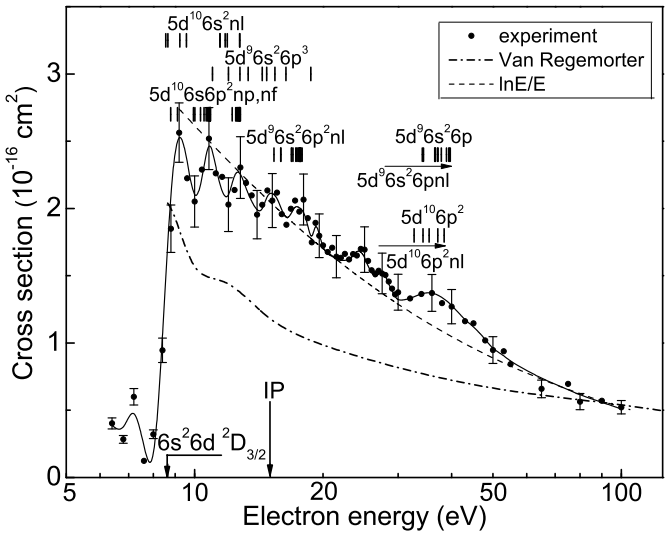

Fig. 2. Electron-impact excitation effective cross section of the Pb^+ ion λ143.4 nm spectral line.

the energy positions of the Pb^+ discrete states and Pb autoionizing states.

It is seen from Figure 2 that the excitation function of the Pb^+ ion resonance line sharply increases at the threshold ($E_{thr} = 8.65$ eV) achieving a maximum at the electron energy $E = 9.2$ eV. At the electron energy $E \geq 5E_{thr}$ it decreases according to the law $\ln E/E$ which is typical for allowed optical transitions.

The excitation function for the resonance line under investigation is non-monotonous with distinct features not only in the near-threshold range, but above the ionization threshold as well. Analysis of the data on the electron configurations and the energy positions of the Pb^+ ionic levels [13] as well as the Pb atomic [14,15] and ionic [16,17] autoionizing states shows that the features are mainly due to the cascade decay of ordinary $5d^{10}6s^2nl$ states as well as autoionizing states to the $5d^{10}6s^26d$ level at the resonance excitation process.

The binding energies of valence and subvalence shells in the Pb^+ ion are comparable. This results in their strong correlation. Therefore, along with the simple spectrum, the lines of which are due to the outer $6p$ electron excitation with the state of $5d^{10}$ and $6s^2$ electrons being unchanged, the Pb^+ ion has a complex spectrum originating from the excitation of the $6s^2$ and $5d^{10}$ shell electrons (see Fig. 3). The simple spectrum consists of relatively small number of lines which, however, are rather intense, while the complex spectrum is characterized by a wide variety of the electronic configurations of energy levels. However, in the energy region below the Pb^+ ionization potential (15.03 eV) there are only levels of $6s6p^2$ configuration, originated from the $6s$ electron excitation, which can not decay to the $6s^26d\ ^2D_{3/2}$ level in accordance with the parity selection rules.

The ion Coulomb attraction favours the excitation of the system "electron + Pb^+" to an infinite set of autoionizing states converging to each ion level. Electronic decay of the autoionizing states with the excited ion formation

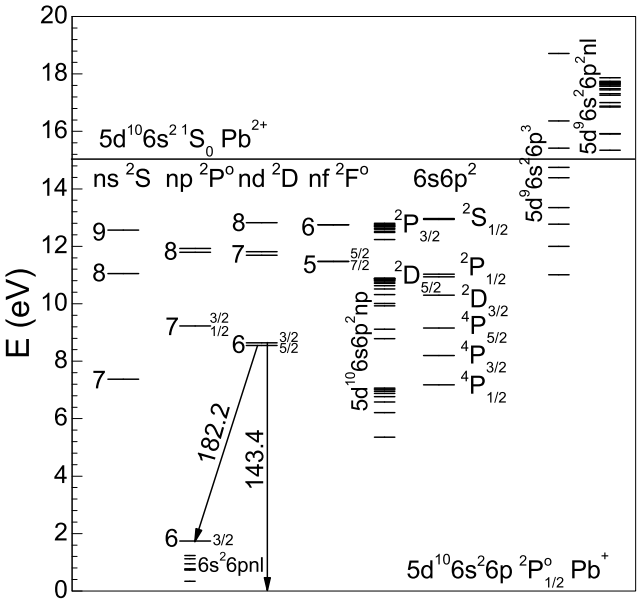

Fig. 3. Energy levels of the Pb^+ ion.

results in resonance excitation of the spectral line under investigation. Relativistic effects as well as intra- and inter-shell correlations considerably affect the autoionizing level widths and result in a variation of the ratio between the probabilities of electronic and radiative decay of the autoionizing states. This fact considerably affects the mechanism of the λ143.4 nm line excitation.

The main channels of formation of the Pb atom (ground state of $5d^{10}6s^26p^2$ configuration) autoionizing states involve $5d \rightarrow 6p$ and $5d \rightarrow np$ ($n \geq 7$) transitions, $6s \rightarrow 6p$ transitions, and transitions within the $6p^2$ configurations [18]. The data on the relevant total photoabsorption spectrum and the ejected-electron spectrum of lead vapour as well as their analysis are given in [14,15]. An important conclusion resulting from the cited works is the absence of two-electron excitations and the stability of the $6p^2$ configuration. Apparently, this is the reason of the very low probability of the $5d^{10}6s^2nln'l'$ autoionizing states formation and their absence in the spectrum of lead vapour.

Each structural feature in the excitation function correlates with specified excited ion states and/or group of autoionizing states (see Fig. 2). Thus, two $5d^{10}6s6p^27p$ autoionizing states of the Pb atom [14,15] are located in the energy range from the excitation threshold of the line under study up to those for the Pb^+ ion $5d^{10}6s^27p$ levels. Starting from the excitation energy of the $5d^{10}6s^27p\ ^2P^o_{1/2}$ level (9.23 eV), the cascades from the $5d^{10}6s^2nl$ multiplets as well as decay of the $5d^{10}6s6p^2np$ ($n \geq 8$) and $5d^96s^26p^3$ autoionizing states [14,15] contribute to the excitation function of the transition under investigation. An interesting fact observed in the experiment is the detection of a structure in the energy range $15 - 50$ eV, i.e. above the ion ionization potential. Analysis shows that this structure can be a result of the decay of the atomic $5d^96s^26p^2np, nf$ autoionizing states [14] as well as the ionic $5d^96s^26pnl$ [16,19] and $5d^{10}6p^2nl$ [17] autoionizing states. Note that the autoionizing states converging to the Pb^+ and Pb^{2+} excited states can decay to the $6s^26d\ ^2D_{3/2}$ level both directly and via intermediate states.

The absolute cross section for the Pb^+ ion resonance line was obtained by normalizing the experimental excitation function to the semi-empirical calculation by the Van-Regemorter formula [20] at 100 eV using the oscillator strength $f = 0.321$ [5]:

$$\sigma_{q_0q_1} = \pi a_0^2 \cdot \frac{8\pi}{\sqrt{3}} \cdot f_{q_0q_1} \cdot \left(\frac{Ry}{\Delta E}\right)^2 \cdot \frac{\gamma(u)}{u+1} \qquad (4)$$

where $\sigma_{q_0q_1}$ is the electron-induced excitation cross section from the lower state q_0 into the upper state q_1, $f_{q_0q_1}$ is the oscillator strength of the transition $q_0 \rightarrow q_1$, a_0 is the Bohr radius, $Ry = 13.6$ eV is the Rydberg energy unit, ΔE is the energy of the transition, $u = \varepsilon/\Delta E - 1$ where ε is the kinetic energy of relative motion between projectile electron and target ion, $\gamma(u)$ is the Gaunt factor chosen on the basis of the experimental data and the theoretical calculations of the effective cross sections, the values of which depending on the value of u are given in the cited work [20].

Note that quantum-mechanical calculations of the electron impact excitation cross section of such multi-electron system as single charged metal ions are complicated and have been performed only for a small number of elements [21]. There are no data on such calculations for the Pb^+ ion available so far. Meanwhile, the semiempirical Van-Regemorter formula is rather widely used because it matches well with the cross sections for optically allowed transitions ($\Delta l = \pm 1$, $\Delta S = 0$) within the same shell at high impact electron energies [22–24]. The accuracy of the excitation cross section calculation depends largely on the gaunt factor value. The values [20] used in our calculation slightly differ from the similar values obtained experimentally or calculated with the use of other approximate formulas [23]. In addition, the semiempirical formula under consideration provides an accuracy up to 50% in the electron energy region $\geq 10E_{thr}$ [24] where the contribution of the cascade transitions into direct excitation of the resonance transition is small and does not exceed 7–10% (see, e.g., Refs. [12,25,26]). The discrepancy between the experimental data and the calculated curve in the energy region $\leq 10E_{thr}$ is due to the fact that the calculation does not consider the contribution of cascade transitions and the resonance contribution of autoionizing states.

The value of the excitation cross section of the resonance transition $6s^26d\ ^2D_{3/2} \rightarrow 6s^26p\ ^2P^o_{1/2}$ (143.4 nm) in the Pb^+ ion is determined to be $(0.5 \pm 0.3) \times 10^{-16}$ cm^2 at the energy 100 eV.

4 Conclusions

The effective cross-section of the electron-impact excitation for the resonance line λ143.4 nm ($6s^26d\ ^2D_{3/2} \rightarrow 6s^26p\ ^2P^o_{1/2}$) in the Pb^+ ion was measured in the range (6–100) eV. Distinct structural features were observed

in the energy dependence of the effective excitation cross section from the threshold up to 50 eV. These features are most likely related to the decay of atomic $5d^{10}6s6p^2np$, $5d^96s^26p^3$, $5d^96s^26p^2np, nf$ and ionic $5d^{10}6p^2nl$, $5d^96s^26pnl$ autoionizing states as well as to the cascade transitions from the ordinary $5d^{10}6s^2nl$ states. Our results show that the resonance excitation is an efficient process at the electron – Pb^+ ion collisions. This is due to the fact that (i) the electron correlations play an essential role in this process because a two-electron transition is possible only provided the electron–electron interaction is taken into account; (ii) in addition to the cascade transitions, some higher-order processes such as the resonance excitation also play an important role.

Unfortunately, no quantum-mechanical theoretical calculations capable of adequate description of the electron-impact excitation mechanism for the Pb^+ ion are available so far. Therefore, to ensure further progress in studying the role of autoionizing states in the effective excitation cross-sections for such complex multielectron ions as Pb^+, quantum-mechanical calculations with the account of both the electron and the radiative decay of autoionizing states are required.

References

1. A. Müller, Adv. At. Mol. Opt. Phys. **55**, 293 (2008)
2. N.R. Badnell, G. Del Zanna, L. Fernández-Menchero, A.S. Giunta, G.Y. Liang, H.E. Mason, P.J. Storey, J. Phys. B **49**, 094001 (2016)
3. J.A. Cardelli, S.R. Federman, D.L. Lambert, C.E. Theodosiou, Astrophys. J. **416**, L41 (1993)
4. D.E. Welty, L.M. Hobbs, J.T. Lauroesch, D.C. Morton, D.G. York, Astrophys. J. **449**, L1 (1995)
5. N. Heidarian, R.E. Irving, A.M. Ritchey, S.R. Federman, D.G. Ellis, S. Cheng, L.J. Curtis, W.A. Furman, Astrophys. J. **808**, 112 (2015)
6. A. Gomonai, E. Ovcharenko, A. Imre, Yu. Hutych, Nucl. Instrum. Methods Phys. Res. B **233**, 250 (2005)
7. E.V. Ovcharenko, A.I. Imre A.N. Gomonai, Yu.I. Hutych, J. Phys. B **43**, 175206 (2010)
8. A.N. Gomonai, Yu.I. Hutych, A.I. Gomonai, Nucl. Instrum. Methods Phys. Res. B **311**, 37 (2013)
9. A. Gomonai, E. Ovcharenko, A. Imre, Yu. Hutych, Publ. Astron. Obs. Belgrade **84**, 119 (2008)
10. S.D. Loch, J.A. Ludlow, M.S. Pindzola, F. Scheuermann, K. Kramer, B. Fabian, K. Huber, E. Salzborn, Phys. Rev. A **72**, 032713 (2005)
11. M.J. Mumma, E.C. Zipf, J. Chem. Phys. **55**, 1661 (1971)
12. W.T. Rogers, J.O. Olsen, G.H. Dunn, Phys. Rev. A **18**, 1353 (1978)
13. J.E. Sansonetti, W.S. Martin, J. Phys. Chem. Ref. Data **34**, 1559 (2005)
14. J.P. Connerade, W.R.S. Garton, M.W.D. Mansfield, M.A.P. Martin, Proc. R. Soc. Lond. A **357**, 499 (1977)
15. V. Pejcev, C.G. Back, K.J. Ross, M. Wilson, J. Phys. B **14**, 4649 (1981)
16. A.J.J. Raassen, Y.N. Joshi, J.-F. Wyart, Phys. Lett. A **154**, 453 (1991)
17. A. Alonso-Medina, C. Colon, A. Zanon, Mon. Not. R. Astron. Soc. **395**, 567 (2009)
18. M.O. Krause, A. Svensson, A. Fahlmann, T.A. Carlson, F. Cerrina, Z. Phys. D **2**, 327 (1986)
19. C. Banahan, C. McGuinness, J.T. Costello, D. Kilbane, J.-P. Mosnier, E.T. Kennedy, G. O'Sullivan, P. van Kampen, J. Phys. B **41**, 205001 (2008)
20. I.I. Sobel'man, L.A. Vainshtein, E.A. Yukov, *Excitation of Atoms and Broadening of Spectral Lines* **15** (Springer, 1995)
21. L. Sharma, A. Surzhykov, R. Srivastava, S. Fritzsche, Phys. Rev. A **83**, 062701 (2011)
22. D.H. Sampson, H.L. Zhang, Phys. Rev. A **45**, 1556 (1992)
23. V. Fisher, V. Bernshtam, H. Golten, Y. Maron, Phys. Rev. A **53**, 2425 (1996)
24. V.I. Fisher Y.V. Ralchenko, V.A. Bernshtam, A. Goldgirsh, Y. Maron, L.A. Vainshtein, I. Bray, H. Golten, Phys. Rev. A **55**, 329 (1997)
25. A.Z. Msezane, J. Phys. B **21**, L61 (1988)
26. G.H. Dunn, D.S. Belic, C. Cisneros, D.H. Crandall, R.A. Falke, D. Gregory, Phys. Rev. A **66**, 032706 (2002)